Engineering Science and Technology, an International Journal 24 (2021) 1134–1143

HOSTED BY

Contents lists available at ScienceDirect

Engineering Science and Technology, an International Journal

journal homepage: www.elsevier.com/locate/jestch

Full Length Article

Sensorless direct torque control based on seven-level torque hysteresis controller for five-phase IPMSM using a sliding-mode observer

Aykut Bıçak, Ayetül Gelen *

Department of Electrical and Electronics Engineering, Bursa Technical University, Bursa, Turkey

ARTICLE INFO

Article history:
Received 20 July 2020
Revised 14 January 2021
Accepted 7 February 2021
Available online 6 March 2021

Keywords:
Direct torque control (DTC)
Five-phase interior PMSM
Torque ripple
Total harmonic distortion (THD)
Sliding-mode observer (SMO)

ABSTRACT

This paper proposes sensorless control of the seven-level torque hysteresis controller (7LTHC) in the direct torque control (DTC) method for five-phase interior permanent magnet synchronous motor (IPMSM). Both torque response and torque ripples of the machine are directly related to the amplitude and location of voltage vectors in the hysteresis DTC method. Additionally, different level torque hysteresis controllers are used to configure a variety of voltage vectors. In this paper, 7LTHC is compared with three-level hysteresis torque controllers (3LTHCs) by using different amplitude voltage vectors to validate the DTC based on the proposed 7LTHC method in Matlab/Simulink environment. Dynamic torque response in the transient operation and low torque ripple and low stator current harmonics in the steady-state operation can be achieved by using the proposed 7LTHC. Furthermore, the speed of IPMSM which is controlled by the DTC based on the proposed 7LTHC is estimated using a sliding-mode observer (SMO) based on sigmoid function and the speed performance is enhanced by combining angle tracking observer (ATO) with the SMO. The simulation results confirm the performance of DTC based on the proposed 7LTHC using the structure of hysteresis DTC and the mathematical model of five-phase IPMSM which uses an SMO for sensorless speed control.
© 2021 Karabuk University. Publishing services by Elsevier B.V. This is an open access article under the CC BY-NC-ND license (http://creativecommons.org/licenses/by-nc-nd/4.0/).

1. Introduction

Multi-phase motors attract considerably more attention comparing to three-phase motors due to their higher efficiency, power density, reliability, lower vibration and torque ripples. Likewise, permanent magnet synchronous motors (PMSM) have superior characteristics such as lower copper losses yielding higher power density, higher efficiency, smaller size, and weight comparing to the induction motors [1,2]. The multi-phase PMSMs, therefore, are preferred to other multi-phase motors in numerous application areas such as electric vehicle drive systems, aerospace and naval propulsion systems, wind turbines, and some other industrial applications [3]. Interior permanent magnet synchronous motors (IPMSM) on the other side gained popularity over surface mounted PMSMs due to their higher torque producing capabilities which combine reluctance and excitation torque [4].

The direct torque control (DTC) method for three-phase induction motor (IM) was first proposed by Takahashi and Noguchi in [5] and implemented by Zhong on three-phase PMSMs [6]. Basically, the DTC method directly controls torque and stator flux by selecting the optimal space vector corresponding to the switching states in each sampling period without performing current control [7,8].

DTC is a simple control method that has numerous advantages such as fast dynamic response, less parameter dependency although it has few drawbacks such as the lack of variable switching frequency and high flux ripples [9]. In DTC method, switching states increases proportionally with number of voltage phase at the inverter output resulting in an increase of the space voltage vector combination. Further, selection of different amplitudes of space voltage vectors minimizes torque ripples and stator flux which are shortcoming of hysteresis controller-based DTC [10]. For example, five phase systems, which have the lowest phase count in the multi-phase systems, provide better adjustment of the torque and the stator flux in contrast to three phase systems [8]. Many other studies [11–13] reports lower torque ripples, eliminated d3-q3 stator flux and harmonic currents and more achievements by utilizing different level torque controllers along with various voltage selections for the IM. In [11], the three-level torque hysteresis controller has applied using different virtual voltage vectors for high-speed and low-speed regions. Similarly, the five-level torque hysteresis controller that used virtual voltage vectors

* Corresponding author at: Bursa Technical University, Dept. of Electrical Electronics Engineering, Mimar Sinan Mah. 16310, Yıldırım-Bursa, Turkey.
E-mail addresses: aykut.bicak@btu.edu.tr (A. Bıçak), ayetul.gelen@btu.edu.tr (A. Gelen).

Peer review under responsibility of Karabuk University.

https://doi.org/10.1016/j.jestch.2021.02.004
2215-0986/© 2021 Karabuk University. Publishing services by Elsevier B.V.
This is an open access article under the CC BY-NC-ND license (http://creativecommons.org/licenses/by-nc-nd/4.0/).

selected according to different speed regions has been presented by [12]. Another study, [13], has proposed a modified five-level hysteresis band for torque controller that using virtual voltage vectors. Finally, it proposed the injection of dither signal in DTC for five-phase IM with a five-level controller using actual voltage vectors [14].

In contrast to IM, there are limited number of studies on PMSM covering the five-phase systems controlled by the DTC based on hysteresis controllers in the literature. Based on the four-level torque controller, the DTC which selects either large or medium vectors depending on the torque error (i.e., the difference between reference and estimated torque values) for the five-phase IPMSMs is proposed in [4]. [15] has presented a two-level torque controller which uses a virtual voltage vector to reduce the effect of d3-q3 stator flux according to its location and to maintain the stator current waveform of five-phase PMSM. [16] has proposed the direct torque model predictive control strategy which can reduce the stator current harmonics and improve the motor torque response for the five-phase IPMSM. A new virtual signal injected MTPA tracking algorithm for DTC based five-phase IPMSMs is proposed in [17].

DTC is a control strategy based on voltage and current models. Rotor position sensor is not required in the DTC voltage model. However, the voltage model is affected by the stator resistance variation and needs to be low pass filtered (LPF) that causes lag to avoid instability. DTC current model requires rotor position feedback, however, while it is not affected by the stator resistance variation. The current model of DTC can be combined with an observer to eliminate the need for a position sensor. The rotor position and speed of the PMSM is estimated using the stator current and voltage waveforms.

Several studies such as extended Kalman filter (EKF) [18,19], Luenberger observer [20], model reference adaptive system (MRAS) [21,22] and phase-locked loop (PLL) observers [23–26] have been presented to improve the performance of sensorless PMSMs. Additionally, the sliding-mode observer (SMO) has been widely used in sensorless PMSM applications. Estimating electrical position of the rotor by using the back electromotive force (EMF), the SMO has many benefits such as their simple structure, fast convergence, robustness, and low sensitivity to parameters [27]. Various SMO approaches have been proposed to analyze their performance in PMSMs [28–30]. Lu et al. implemented the load torque identification SMO which contains an LPF used as the load torque observer and the signum function is also replaced with a saturation function [28]. In [29], the saturation function is used to achieve sensorless control of vector controlled five-phase surface-mounted PMSM with SMO. An SMO which utilizes the arctangent method to estimate rotor electrical position has been presented in [30] for five-phase IPMSMs controlled by space vector modulation technique.

This paper analyzes effects of different amplitude voltage vectors on the torque ripple, torque response and stator current distortion in the transient and the steady states for a five-phase IPMSM which is implemented using the DTC based on a hysteresis controller. We started with a three-level controller for small, medium, and large voltage vectors. To obtain a fast, dynamic torque response in the transient state, eliminate stator harmonics and reduce torque ripples in the steady-state, the seven-level torque hysteresis controller (7LTHC) is proposed. The main contributions of the paper are listed as follows: 1) The 7LTHC utilizing the proposed voltage vector selection look-up table regulates the torque ripple, improves torque response, and reduces current distortions of five-phase IPMSMs 2) A phase-locked loop (PLL) based angle tracking observer (ATO) along with the SMO is implemented to sensorless control an IPMSM with the proposed 7LTHC method without using a position sensor. The sigmoid function-based SMO combined with ATO eliminates the use of both the LPF causing phase delay and the arctangent method causing oscillations. The effect of DTC based on the proposed 7LTHC method is illustrated in simulations for both position sensored and sensorless operation.

The paper is organized as follows. Section 2 presents the mathematical model of five-phase PMSM. Principle of DTC is described in Section 3. Section 4 describes the selection of voltage vectors for 7LTHC. Sigmoid function-based SMO combined with ATO is presented in section 5. The simulation results of the proposed 7LTHC method are given in section 6. Finally, the section 7 concludes the paper.

2. Mathematical model of five-phase PMSM

To simplify the five-phase PMSM modeling, the five-phase system (abcde) is transformed to an orthogonal (dq) reference frame. Then the five-phase PMSM model in the rotating (dq) reference frame is as the following [15]:

$$\left[v_{dq0}\right] = \left[T_{dq0}(\theta)\right]\left[v_{abcde}\right] \tag{1}$$

The transformation matrix is written as:

$$[T_{dq0}] = \left(\frac{2}{5}\right)\begin{bmatrix} \cos(\theta) & \cos\left(\theta-\frac{2\pi}{5}\right) & \cos\left(\theta-\frac{4\pi}{5}\right) & \cos\left(\theta+\frac{4\pi}{5}\right) & \cos\left(\theta+\frac{2\pi}{5}\right) \\ -\sin(\theta) & -\sin\left(\theta-\frac{2\pi}{5}\right) & -\sin\left(\theta-\frac{4\pi}{5}\right) & -\sin\left(\theta+\frac{4\pi}{5}\right) & -\sin\left(\theta+\frac{2\pi}{5}\right) \\ \frac{1}{2} & \frac{1}{2} & \frac{1}{2} & \frac{1}{2} & \frac{1}{2} \end{bmatrix} \tag{2}$$

The stator flux equations in the dq rotating reference frame are:

$$\lambda_{ds} = L_d i_{ds} + \lambda_m \tag{3}$$

$$\lambda_{qs} = L_q i_{qs} \tag{4}$$

where L_d and L_q are the dq axis inductances, i_{ds} and i_{qs} are the dq axis stator currents. λ_m is the permanent magnet flux linkage. The stator voltage equations in the dq rotating reference frame are given as:

$$V_{ds} = r_s i_{ds} - \omega_r \lambda_{qs} + \frac{d\lambda_{ds}}{dt} \tag{5}$$

$$V_{qs} = r_s i_{qs} + \omega_r \lambda_{ds} + \frac{d\lambda_{qs}}{dt} \tag{6}$$

where V_{ds} and V_{qs} are the dq axis stator voltages. r_s, ω_r are the stator resistance and rotor electrical speed, respectively. The electromagnetic torque and mechanical torque are formulated as:

$$T_e = \left(\frac{5}{2}\right)P\left(\lambda_m i_{qs} + (L_d - L_q) i_{ds} i_{qs}\right) \tag{7}$$

$$T_e = J\left(\frac{d\omega_m}{dt}\right) + T_L + B\omega_m \tag{8}$$

$$\left(\frac{d\theta_r}{dt}\right) = \omega_r = P\omega_m \tag{9}$$

where T_e is the electromagnetic torque, J is the inertia of the rotor, T_L is the motor load torque, B is the viscous friction coefficient, ω_m is the rotor mechanical speed, and θ_r is the rotor electrical position, respectively. P is the number of pole pairs. The first term of the electromagnetic torque is the excitation torque and the second one is the reluctance torque in (7). IPMSM combines the excitation torque and the reluctance torque, whereas surface-mounted PMSM produces only the excitation torque since the d and q axis inductance values are equal.

3. Principle of DTC

DTC method provides an optimal selection of the space voltage vectors which consist of the inverter switching states according to the errors between the actual and reference values of flux and torque in each sampling period by using the two separate hysteresis controllers and the position information. The flux controller consists of a two-level hysteresis band, whereas the torque controller can be configured from a two-level to seven-level hysteresis band for five-phase systems.

Estimations of the amplitude and direction of stator flux linkage is needed for optimal voltage vector selection. The estimation of stator flux utilizes either the voltage model or the current model. The voltage model requires fewer parameters comparing to the current model. In order to avoid instability in the motor drive system, the voltage model utilizes an LPF instead of the pure integrator which could increase the complexity of the controller [31]. The current model, on the other hand, needs the rotor position information. In this paper, the current model is used as the rotor position estimator because of its simple structure. Therefore, an SMO is added to the DTC control system based on the current model to avoid using rotor position sensor.

The estimated torque and stator flux linkage, and the sector can be derived with α-axis and β-axis stator flux linkage components in the stationary reference frame. Stator flux linkage can be calculated by (10), (11) using phase currents and the dc bus voltage measurements of the voltage model.

$$\lambda_\alpha = \int (v_\alpha - r_s i_\alpha) dt \tag{10}$$

$$\lambda_\beta = \int (v_\beta - r_s i_\beta) dt \tag{11}$$

Stator flux linkage can also be calculated with the Park to Clarke transformation using the reference frame currents and the rotor position for the current model as given by (12).

$$\begin{bmatrix} \lambda_\alpha \\ \lambda_\beta \\ \lambda_0 \end{bmatrix} = \begin{bmatrix} \cos\theta & -\sin\theta & 0 \\ \sin\theta & \cos\theta & 0 \\ 0 & 0 & 1 \end{bmatrix} \begin{bmatrix} \lambda_d \\ \lambda_q \\ \lambda_0 \end{bmatrix} \tag{12}$$

The amplitude of stator flux linkage estimator can be expressed as:

$$|\lambda_{est}| = \sqrt{\lambda_\alpha^2 + \lambda_\beta^2} \tag{13}$$

The angle of the stator flux vector determines the sector. It can be derived as:

$$\angle\lambda_{est} = \theta = \tan^{-1}\left(\frac{\lambda_\beta}{\lambda_\alpha}\right) \tag{14}$$

The torque estimator can be given by:

$$T_{est} = \left(\frac{5}{2}\right) P(\lambda_\alpha i_\beta - \lambda_\beta i_\alpha) \tag{15}$$

The two-level inverter, which has two legs consisting of two switches, takes the value 1 when the upper switch is on and the lower switch is off and 0 for other switch states. In this case, there are 2^n different space voltage vectors for a two-level n-phase inverter. Therefore, the phase voltages can be expressed as a matrix according to switching states of the two-level five-phase voltage source inverter (VSI).

$$\begin{bmatrix} V_a \\ V_b \\ V_c \\ V_d \\ V_e \end{bmatrix} = \left(\frac{V_{dc}}{5}\right) \begin{bmatrix} 4 & -1 & -1 & -1 & -1 \\ -1 & 4 & -1 & -1 & -1 \\ -1 & -1 & 4 & -1 & -1 \\ -1 & -1 & -1 & 4 & -1 \\ -1 & -1 & -1 & -1 & 4 \end{bmatrix} \begin{bmatrix} S_a \\ S_b \\ S_c \\ S_d \\ S_e \end{bmatrix} \tag{16}$$

where V_{dc} is the inverter dc-link voltage, S_a, S_b, S_c, S_d, S_e are the switching states of the two-level five-phase VSI. Besides, the five-phase inverter has 32 space voltage vectors which 30 of them are active and 2 are zero. These voltage vectors are divided into four categories according to amplitude sets: large, medium, small, and zero. The ratios of the active voltage vector amplitudes from the smallest set to the largest set are 1:1.618:1.618^2, respectively. Each set contains 10 active voltage vectors, while there is an angle of π/5 rad between the adjacent vectors. Additionally, the vector space is divided equally into 10 sectors of π/5 rad [10]. There are three active voltage vectors which have different amplitudes located in the same direction of each sector, while zero voltage vectors are located at the origin of the voltage plane. Thus, V_0 and V_{31} are called zero voltage vectors that corresponding to the case that all switches take the value of 0 or 1. Fig. 1 shows the voltage vectors and switching states in dq sub-space for the two-level five-phase VSI. Additionally, the sectors consist of a vector plane are divided into ten parts as depicted in Fig. 1.

The voltage vectors are applied according to the torque and stator flux errors, i.e., the difference between their reference and the estimated values. The flux hysteresis controller consists of a two-level hysteresis band. Stator flux comparator ($d\lambda$ = 1) represents the required increment in the actual flux, whereas ($d\lambda$ = 0) represents the required decrement in the actual flux. However, the torque hysteresis controller can be configured up to seven-level hysteresis band for five-phase systems. Table 1 shows the zero voltage vectors employed when the torque controller (dT) is 0 which implies the torque error is in the center level. If torque error lies between the inner level HB_1 and HB_2 or -HB_1 and -HB_2, then the dT is 1 or −1, respectively. Small voltage vectors are uti-

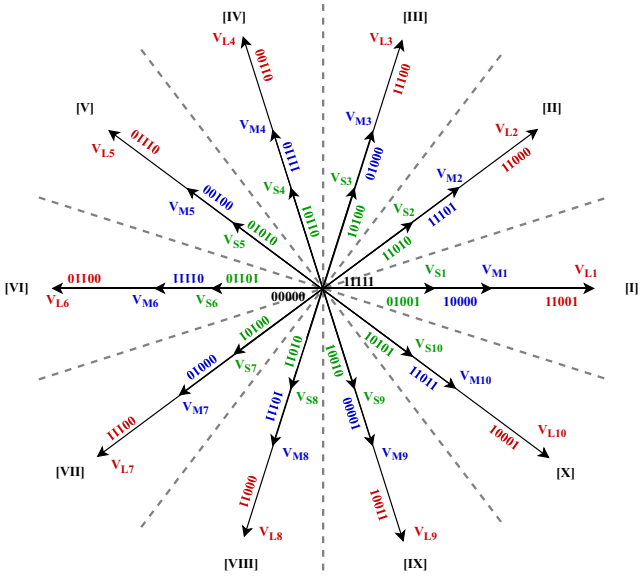

Fig. 1. The voltage vectors, switching states and sectors in dq sub-space.

Table 1
Active voltage-vector lookup table.

$d\lambda$	dT	Sector									
		I	II	III	IV	V	VI	VII	VIII	IX	X
1	3	V_{L3}	V_{L4}	V_{L5}	V_{L6}	V_{L7}	V_{L8}	V_{L9}	V_{L10}	V_{L1}	V_{L2}
	2	V_{M3}	V_{M4}	V_{M5}	V_{M6}	V_{M7}	V_{M8}	V_{M9}	V_{M10}	V_{M1}	V_{M2}
	1	V_{S3}	V_{S4}	V_{S5}	V_{S6}	V_{S7}	V_{S8}	V_{S9}	V_{S10}	V_{S1}	V_{S2}
	0	V_0	V_{31}	V_0	V_{31}	V_0	V_{31}	V_0	V_{31}	V_0	V_{31}
	−1	V_{S9}	V_{S10}	V_{S1}	V_{S2}	V_{S3}	V_{S4}	V_{S5}	V_{S6}	V_{S7}	V_{S8}
	−2	V_{M9}	V_{M10}	V_{M1}	V_{M2}	V_{M3}	V_{M4}	V_{M5}	V_{M6}	V_{M7}	V_{M8}
	−3	V_{L9}	V_{L10}	V_{L1}	V_{L2}	V_{L3}	V_{L4}	V_{L5}	V_{L6}	V_{L7}	V_{L8}
0	3	V_{L4}	V_{L5}	V_{L6}	V_{L7}	V_{L8}	V_{L9}	V_{L10}	V_{L1}	V_{L2}	V_{L3}
	2	V_{M4}	V_{M5}	V_{M6}	V_{M7}	V_{M8}	V_{M9}	V_{M10}	V_{M1}	V_{M2}	V_{M3}
	1	V_{S4}	V_{S5}	V_{S6}	V_{S7}	V_{S8}	V_{S9}	V_{S10}	V_{S1}	V_{S2}	V_{S3}
	0	V_{31}	V_0	V_{31}	V_0	V_{31}	V_0	V_{31}	V_0	V_{31}	V_0
	−1	V_{S8}	V_{S9}	V_{S10}	V_{S1}	V_{S2}	V_{S3}	V_{S4}	V_{S5}	V_{S6}	V_{S7}
	−2	V_{M8}	V_{M9}	V_{M10}	V_{M1}	V_{M2}	V_{M3}	V_{M4}	V_{M5}	V_{M6}	V_{M7}
	−3	V_{L8}	V_{L9}	V_{L10}	V_{L1}	V_{L2}	V_{L3}	V_{L4}	V_{L5}	V_{L6}	V_{L7}

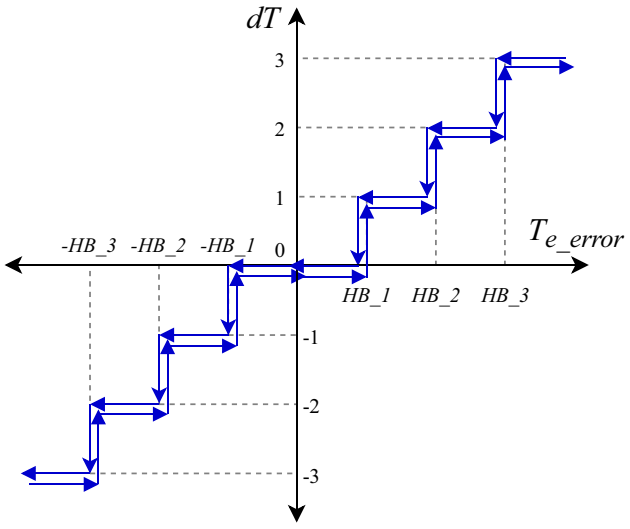

Fig. 2. Seven-level torque hysteresis controller.

lized since they have a slow dynamic response and low torque ripple in the inner level. If torque error is in the middle-level HB_2 and HB_3 or -HB_2 and -HB_3, then the dT is 2 or −2, respectively. Medium voltage vectors are employed as they have medium dynamic response and medium torque ripple in the medium level. If torque error is greater than HB_3 or less than -HB_3, then the dT is 3 or −3, respectively. Large voltage vectors are employed which have a fast-dynamic response and larger torque ripple for torque error that lies in the outer level. The scheme of operation of the 7LTHC according to hysteresis bandwidth is shown in Fig. 2.

In this paper, the ratios of hysteresis torque controller bandwidths are selected based on the ratios of active voltage vectors' magnitudes as 1:1.618: 1.618^2, from the smallest one to the largest one, respectively.

4. Selection of voltage vectors

The voltage vectors are employed for either decreasing or increasing the torque and the stator flux. For example, suppose that the stator flux linkage vector has been rotating in counterclockwise direction and is located in the first sector. Voltage vectors V_{X2} or V_{X3} can be used to increase both the electromagnetic torque and the stator flux (TI, FI). Voltage vectors V_{X4} or V_{X5} must

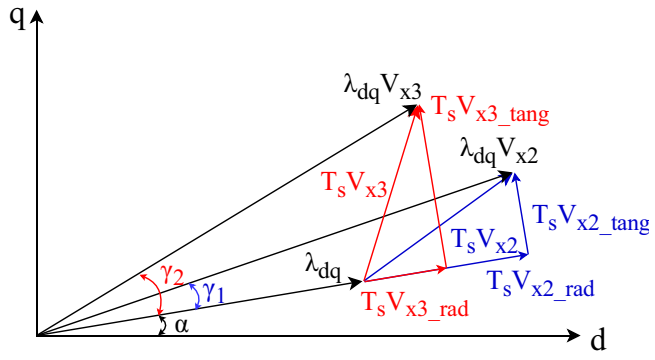

Fig. 3. The effect of using different voltage vectors on stator flux-linkage and electromagnetic torque for sector I.

be used to decrease the stator flux while increasing the electromagnetic torque (TI, FD), and the V_{X9} or V_{X10} vectors must be used for the opposite situation (TD, FI). If both the flux and the torque are needed to decrease (TD, FD), then the voltage vectors V_{X7} or V_{X8} must be selected. V_X represents the amplitude of voltage vectors as small, medium, and large. The large voltage vector V_L provides a faster response on changing torque and flux. Its followed by the medium voltage vector V_M. However, the small voltage vector V_S generates the lowest rate of change in terms of response for both the torque and the flux.

Additionally, each voltage vector is split into two components, the tangential and the radial components in the dq reference frame. The stator flux amplitude is affected by the radial component, whereas the electromagnetic torque response is affected by the tangential component of the voltage vector. Fig. 3 shows the effect of the radial components and the tangential components of voltage vectors V_{X2} and V_{X3} when the stator flux is in the first sector. V_{X2} voltage vector has a larger radial component than V_{X3} has, while V_{X3} voltage vector has a larger tangential component than V_{X2} has. Therefore, V_{X3} produces faster torque response comparing to V_{X2}, while V_{X2} performs better stator flux control. Similarly, V_{X4}, V_{X8}, and V_{X9} produce fast responses like V_{X3} to increment or decrement reference torque for sector I. Therefore, this vector group can be called the fast torque response vectors (V_{XF}) while the other vector group can be described as the slow torque response vector (V_{XS}). Six active voltage vector groups classified by their impact on the torque response and ripple can mentioned: V_{SS}, V_{SF}, V_{MS}, V_{MF}, V_{LS}, V_{LF}. These voltage vector groups are used in various combinations that enabling torque control strategies with different

levels of the hysteresis controller. These groups can be combined with zero voltage vectors to decrease the applied number of vectors especially when it is necessary to reduce the torque.

The large voltage vector has a fast torque response in the transient state, while it increases the torque ripple in the steady state. The medium and the small voltage vectors reduce the torque ripple in the steady state; however, they have slower torque response comparing to the large voltage vector. We propose a 7LTHC to improve the dynamic torque response by using the large voltage vector and to reduce the torque ripple by using the small and the medium voltage vectors. The proposed 7LTHC which uses the fast torque response vectors (V_{SF}, V_{MF}, V_{LF}) is shown in Table 1. The proposed method enhances the torque response and reduces the current harmonic distortion for each vector amplitude.

5. Design of SMO for the IPMSM

The model of IPMSM in the αβ stationary reference frame is designed as using the equivalent EMF [27].

$$\frac{d}{dt}\begin{bmatrix} i_\alpha \\ i_\beta \end{bmatrix} = \frac{1}{L_q}\begin{bmatrix} v_\alpha \\ v_\beta \end{bmatrix} - \frac{r_s}{L_q}\begin{bmatrix} i_\alpha \\ i_\beta \end{bmatrix} - \frac{1}{L_q}\begin{bmatrix} e_\alpha \\ e_\beta \end{bmatrix} \tag{17}$$

where i_α, i_β, v_α, v_β and e_α, e_β are the current, voltage, and the back-EMF in the αβ stationary reference frame, respectively.

The conventional SMO is designed using IPMSM equations as:

$$\frac{d}{dt}\begin{bmatrix} \hat{i}_\alpha \\ \hat{i}_\beta \end{bmatrix} = \frac{1}{L_q}\begin{bmatrix} v_\alpha \\ v_\beta \end{bmatrix} - \frac{r_s}{L_q}\begin{bmatrix} \hat{i}_\alpha \\ \hat{i}_\beta \end{bmatrix} - \frac{k_{SMO}}{L_q}\begin{bmatrix} sign(\hat{i}_\alpha - i_\alpha) \\ sign(\hat{i}_\beta - i_\beta) \end{bmatrix} \tag{18}$$

where $\hat{i}$ denotes the estimated values, and k_{SMO} represents the constant observer gain.

The conventional SMO using signum function causes the chattering effect in the system. A low pass filter (LPF) is usually combined with the conventional SMO to reduce the chattering effect. However, since LPFs cause phase delay [32,33], the signum function can also be replaced by the sigmoid function to reduce the chattering effect. The sigmoid function is defined as:

$$H\left(\tilde{i}\right) = \left(\left(\frac{2}{(1+e^{-a\,\tilde{i}})}\right) - 1\right) \tag{19}$$

where $\tilde{i}$ denotes the estimation error between observed current and actual current as defined in (20), and a represents the constant parameter of the sigmoid function regulating the slope.

$$\begin{bmatrix} \tilde{i}_\alpha \\ \tilde{i}_\beta \end{bmatrix} = \begin{bmatrix} \hat{i}_\alpha - i_\alpha \\ \hat{i}_\beta - i_\beta \end{bmatrix} \tag{20}$$

Thus, the equation of observer can be rewritten as:

$$\frac{d}{dt}\begin{bmatrix} \hat{i}_\alpha \\ \hat{i}_\beta \end{bmatrix} = \frac{1}{L_q}\begin{bmatrix} v_\alpha \\ v_\beta \end{bmatrix} - \frac{r_s}{L_q}\begin{bmatrix} \hat{i}_\alpha \\ \hat{i}_\beta \end{bmatrix} - \frac{k_{SMO}}{L_q}\begin{bmatrix} H(\tilde{i}_\alpha) \\ H(\tilde{i}_\beta) \end{bmatrix} \tag{21}$$

The stability of the observer is verified using the Lyapunov function which is defined as V.

$$V = \frac{1}{2}(\tilde{i}_\alpha^2 + \tilde{i}_\beta^2) \tag{22}$$

The derivative of the Lyapunov function with respect to time is given as:

$$\frac{dV}{dt} = \left(\frac{d\tilde{i}_\alpha}{dt}\right)\tilde{i}_\alpha + \left(\frac{d\tilde{i}_\beta}{dt}\right)\tilde{i}_\beta \leqslant 0 \tag{23}$$

The derivative of the Lyapunov function must be negative to satisfy the stability condition, i.e., the estimated current will converge to its actual value until the error reaches zero. Therefore, k_{SMO} must be selected large enough according to (24).

$$k_{SMO} > \max(|e_\alpha|, |e_\beta|) \tag{24}$$

k_{SMO} can ensure the asymptotical stability of sliding motion. Once the system reaches the sliding surface, it will stay on the surface. After then:

$$\begin{bmatrix} \tilde{i}_\alpha \\ \tilde{i}_\beta \end{bmatrix} = S(X) = \frac{d}{dt}S(X) = 0 \tag{25}$$

The rotor electrical position is estimated using the negative arctangent method based on the back-EMF, then the observed rotor electrical position is obtained as:

$$\hat{\theta}_r = -\tan^{-1}\left(\frac{e_\alpha}{e_\beta}\right) = -\tan^{-1}\left(\frac{k_{SMO}H(\tilde{i}_\alpha)}{k_{SMO}H(\tilde{i}_\beta)}\right) \tag{26}$$

The arctangent method causes oscillations in the estimated rotor position [34]. To solve this problem, in this paper, the estimated rotor electrical position is obtained from the SMO which is combined with the ATO based on the PLL. Fig. 4 shows the scheme of the SMO combined with the ATO.

Driven by sensorless DTC based on the proposed 7LTHC method using the SMO, the block diagram of the five-phase IPMSM is given in Fig. 5. The five-phase voltage of the VSI is transformed from the five-phase to the rotating reference frame. The estimated torque (T_{est}), stator flux linkage (λ_{est}), and sector are obtained by the estimation block of DTC. Also, The SMO based on the back-EMF model combined with ATO estimates the electrical position of the rotor. The estimated rotor electrical position ($\hat{\theta}_r$) obtained by the obser-

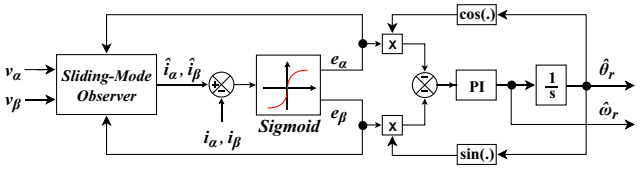

Fig. 4. Block diagram of sigmoid function-based sliding-mode observer combined with angle tracking observer.

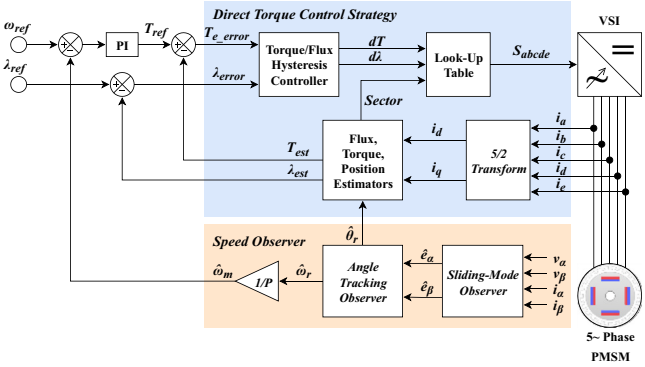

Fig. 5. Control block diagram of sensorless drive system of DTC based on the proposed 7LTHC using the SMO.

ver is transformed into the estimated rotor mechanical speed ($\hat{\omega}_m$) as rpm. Thus, the speed error can be obtained by the difference between estimated rotor mechanical speed ($\hat{\omega}_m$) and reference speed (ω_{ref}). The speed error ($\tilde{\omega}_m$) that is obtained is corrected by implementing the proportional-integral (PI) controller in order to generate the reference torque (T_{ref}) of the motor. Therefore, the reference torque (T_{ref}) output from the PI controller and the reference stator flux (λ_{ref}) are compared with their own estimated values. The estimated values are subtracted from the reference values to obtain the corresponding errors. Both respective errors pass through their own hysteresis controller. The required voltage vector is determined according to the stator flux vector position and the digital outputs of the torque and the stator flux hysteresis controllers (dT, $d\lambda$), respectively, using the lookup table as shown in Table 1. The switching states of the selected actual voltage vector are applied to five-phase IPMSM by the two-level five-phase VSI.

6. Simulation results

The performance of DTC based on the proposed 7LTHC method for five-phase PMSM is analyzed in terms of both actual speed and observed speed using Matlab/Simulink environment. The parameters of the five-phase PMSM are given in Table 2 [35]. The inverter dc-link voltage is 120 V. The sampling time of the simulation is set to 25 μs. Furthermore, the values of the PI controller which obtained by manual tuning is designed so that the actual torque value immediately tracks to the reference torque value during load changes. Therefore, the integral gain (K_i) and the proportional gain (K_p) are specified as 40 and 10, respectively.

The torque hysteresis band is set to ± 0.1 Nm of the reference torque for the three-level controller which is applied small, medium, and large voltage vectors, separately to show the effect of vectors at the same bandwidth. If the bandwidth of the hysteresis controller doesn't proper with the magnitude of the voltage vector, the torque is controlled exceed the hysteresis band by the voltage vector. Unlike, inner level (HB_1), middle level (HB_2), and outer level (HB_3) of the torque hysteresis bands of the seven-level controller are set to ± 0.1 Nm, ± 0.1618 Nm, and ± 0.2618 Nm, respectively. The magnitude of bandwidths is adjusted to proportional with the amplitude of voltage vectors. Moreover, the flux hysteresis band is set to ± 0.00025 Wb of the reference flux for all methods.

6.1. Dynamic performance

Firstly, the proposed 7LTHC using the fast torque response vectors is compared with the three-level hysteresis torque controller (3LTHC) that uses different voltage vector groups in terms of torque response in transient state. The external step load torque (reference torque) which reaches from 0 Nm to 2 Nm is applied to the motor at time t = 0.5 s for comparing the performance of the three-level controllers as shown in Fig. 6. The torque response time is 0.13 ms when applied to the large-fast torque response vectors

Table 2
Parameters of Five-Phase IPMSM.

Symbol	Parameter	Value
P	number of pole pairs	2
L_d	d-axis inductance	0,381 mH
L_q	q-axis inductance	0,956 mH
r_s	stator resistance	0,21 Ω
λ_m	permanent magnet flux linkage	0,043 Wb
B	viscous friction coefficient	0,001 Nm/(rad/s)
J	inertia of the rotor	0,015 kg.m^2

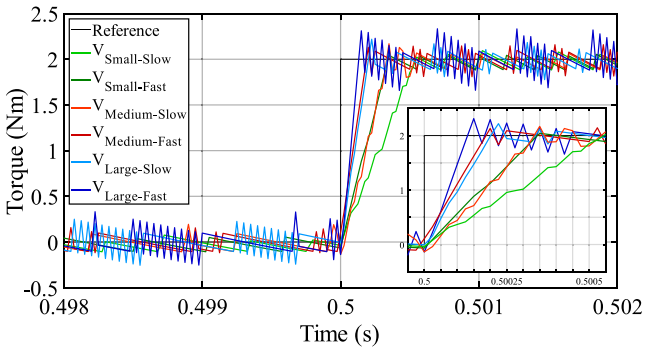

Fig. 6. Comparison of torque dynamic response of different voltage vectors for step change of reference torque from 0 Nm to 2 Nm at 3LTHC.

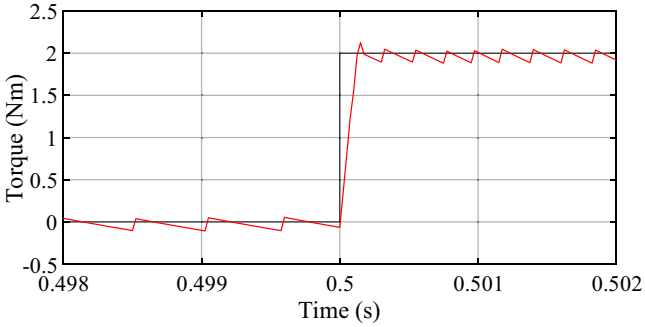

Fig. 7. Dynamic response of the proposed 7LTHC for step change of reference torque from 0 Nm to 2 Nm.

(V_{LF}) that have the best performance in terms of dynamic response time. On the other hand, the torque response time is 0.544 ms when selected small-slow torque response vectors (V_{SS}). The response time of the proposed 7LTHC that uses V_{LF} in transient state operation has 0.129 ms which is the best response time, as shown in Fig. 7.

6.2. Steady-state performance

Performances of steady-state are analyzed according to actual speed of the motor without using observer. Fig. 8 shows the torque ripple of the 3LTHC that using different voltage vector groups for the steady-state operation in various actual speed conditions for the load torque fixed to 2 Nm. It is seen that the torque ripple is increased with the increase in the magnitude of voltage vector. The fast torque response vectors have also increased the ripple of torque compared to slow response vector groups. The torque ripple

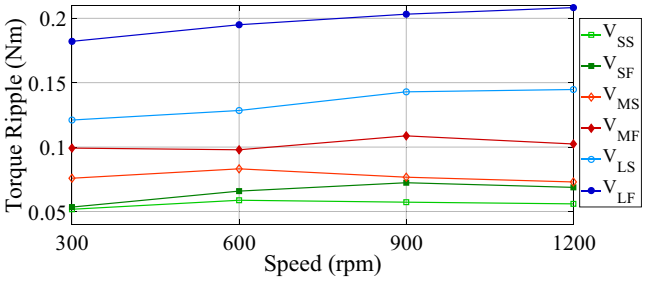

Fig. 8. Comparison of torque ripple for different voltage vector groups at various speed and load torque of 2 Nm at three-level controllers.

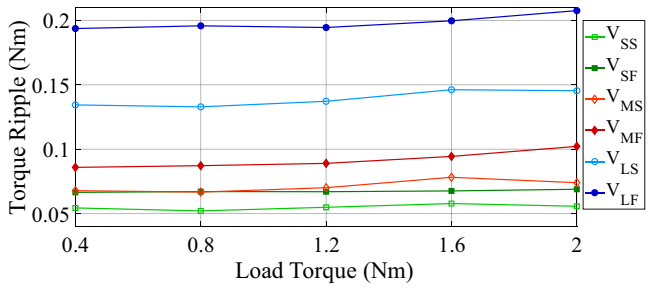

Fig. 9. Comparison of torque ripple for different voltage vector groups at various load torque and reference speed of 1200 rpm at three-level controllers.

equation which is derived by using the root mean square error [36] is given by:

$$T_{e_{ripple}} = \sqrt{\frac{1}{n}\sum_{i=1}^{n}\left(T_e(i) - T_{e_{avg}}\right)^2} \tag{27}$$

where $T_e(i)$ and T_{eavg} are the instant torque value and the average value of torque, respectively, also n represents the number of samples.

As seen in Fig. 8 and Fig. 9, the torque ripple of three-level controllers is almost the same value both at varying speed conditions with fixed load and varying load conditions with fixed speed. Besides, the current harmonics have reduced at increased load torque and fix speed conditions as shown in Fig. 10. However, it is almost the same value at increased speed and fixed load as depicted in Fig. 11. The groups of small vectors (V_{SS} and V_{SF}) better reduce to ripple of torque, while the groups of fast vectors (V_{SF} and V_{MF}) better eliminate the current harmonics. For this reason, the proposed 7LTHC is compared with the small vector groups (V_{SS}, V_{SF}) of the 3LTHC in terms of torque ripple while the proposed 7LTHC is compared with the small-fast and the medium-fast vector

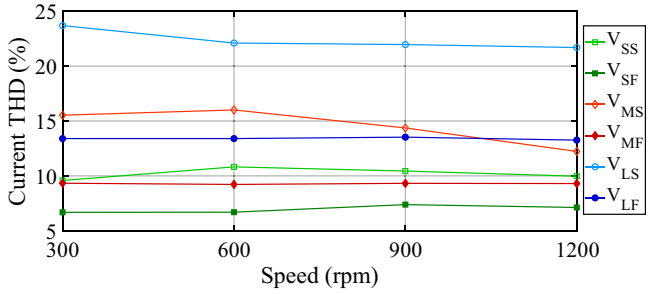

Fig. 10. Comparison of stator current THD for different voltage vector groups at various speed and load torque of 2 Nm at three-level controllers.

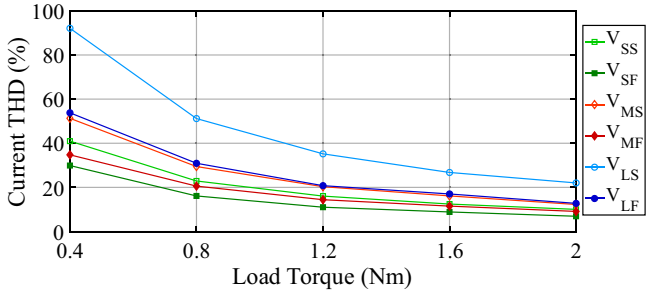

Fig. 11. Comparison of stator current THD for different voltage vector groups at various load torque and reference speed of 1200 rpm at three-level controllers.

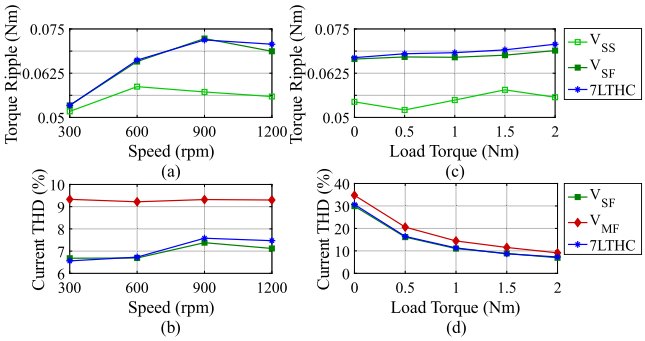

Fig. 12. Comparison of performance between the proposed 7LTHC and 3LTHC (VSS, VSF, VMF). (a) torque ripple for varying speed in 7LTHC, VSS, and VSF schemes, and (b) current THD for varying speed in 7LTHC, VSF, and VMF schemes, and (c) torque ripple for varying load torque in 7LTHC, VSS, and VSF schemes, and (d) current THD for varying load torque in 7LTHC, VSF, and VMF schemes.

groups (V_{SF}, V_{MF}) of the 3LTHC in terms of current distortion, and the results are presented in Fig. 12.

The proposed 7LTHC has reduced the torque ripple as much as the small-fast vectors under both the same load condition which is 2 Nm and the same speed condition which is 1200 rpm, as depicted in Fig. 12(a) and (c). Also, the proposed method that applied the small-fast vectors (V_{SF}) in steady-state operation has total harmonic distortion as less as a three-level controller that applied the V_{SF}, as shown in Fig. 12(b) and (d). Similarly, the proposed 7LTHC method has almost the same values with V_{SF} in 3LTHC both current harmonics and torque ripple at various load and fixed base speed which is 1200 rpm. Hence, DTC based on the proposed 7LTHC band provides fast dynamic torque response while reduces to the torque and stator current ripples as much as small-fast vectors in the steady-state operation. Besides, the proposed 7LTHC avoids applying V_{SS} that causing an extreme increasing the current harmonics even if it reduces of the torque ripples.

The dynamic performance of the proposed 7LTHC method is affected by the PI controller that generates the reference torque for the motor. Therefore, the V_{LF} groups are mostly applied and the V_{MF} groups are rarely applied in the transient states. Similarly, V_{MF} groups are rarely applied in the steady-state operation, contrary to V_{SF} groups.

6.3. Performance of 7LTHC control strategy using SMO

To verify the correctness and robustness of the SMO combined with ATO has implemented to the 7LTHC control strategy. The observer gain (k_{SMO}) and constant the parameter of sigmoid function (a) are set to 125 and 0.1, respectively.

The reference speed is increased from standstill to 120 rpm which 10% of base speed, and then is changed from 120 rpm to 600 rpm which 50% of base speed, and finally is accelerated from 600 rpm to 1200 rpm which is base speed. The motor run under no-load torque condition in this test. The change in actual speed (ω_{act}) and estimated speed (ω_{est}) according to reference speed (ω_{ref}) is shown in Fig. 13. Moreover, Fig. 13 shows the zoomed-in view of each speed value. The ripple of estimated speed is almost the same at 600 rpm and 1200 rpm that is 2.48 rpm and 2.47 rpm, respectively. However, the ripple of speed is 6.08 rpm at 120 rpm as the biggest value in steady-state condition.

Fig. 14 shows the waveform of the speed estimation error. In steady-state conditions, the speed error between actual and estimated speed is bounded between +38 rpm and −20 rpm at 120 rpm. At 600 rpm, the error has changed between +5 rpm and −8 rpm. The error has also changed between 3 rpm and −4 rpm

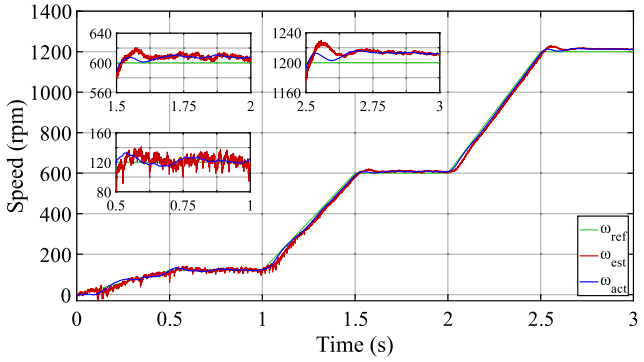

Fig. 13. Estimated and actual mechanical speeds for the proposed 7LTHC method under no-load condition using SMO.

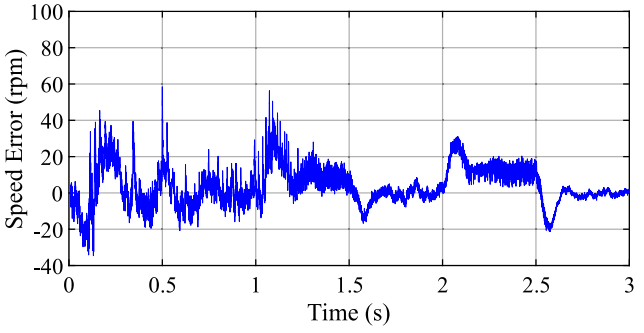

Fig. 14. Estimated rotor mechanical speed error with the SMO.

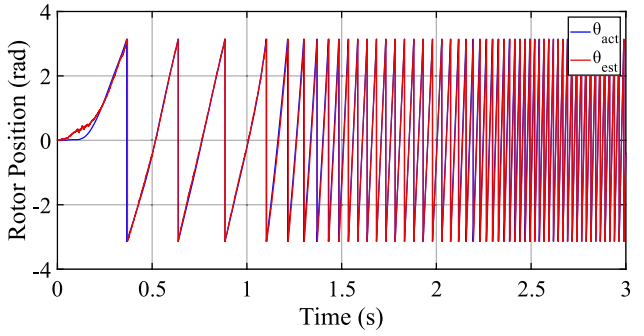

Fig. 15. Estimated and actual rotor electrical position.

at 1200 rpm. The maximum speed error is 58 rpm in the transient condition.

Fig. 15 shows the comparison of the estimated rotor electrical position with the actual rotor electrical position. The applied SMO combined with ATO has small oscillations and some delay while the observer has good accuracy and tracking performance.

The position error between the estimated rotor electrical position (θ_{est}) and the actual rotor electrical position (θ_{act}) is displayed in Fig. 16. The position estimation error various around 0.1 rad at 120 rpm. It is around 0.05 rad and 0.04 rad at 600 rpm and 1200 rpm, respectively. The maximum position estimation error is around 0.39 rad when speed is changed from 0 rpm to 120 rpm for transient state.

Fig. 17 shows the performance of electromagnetic torque ripple of the proposed 7LTHC method according to both measured speed and observed (estimated) speed under 2 Nm at 1200 rpm in

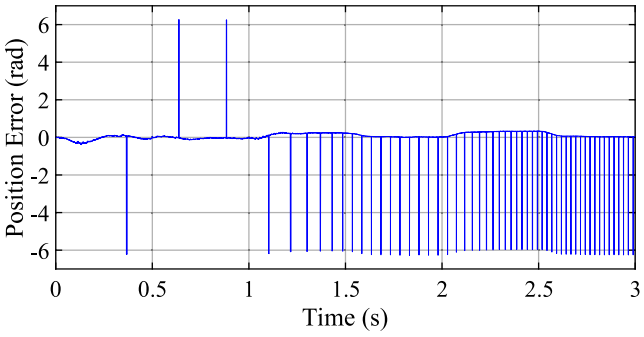

Fig. 16. Errors between estimated and actual rotor position.

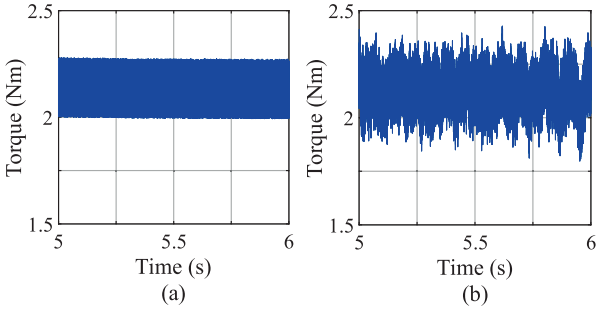

Fig. 17. Actual torque waveform for the proposed 7LTHC method under 2 Nm. (a) with measured speed (b) with observed speed.

steady-state condition. The torque ripple is 0.072 when controlled according to the measured speed, while the torque ripple is 0.089 according to the observed speed, as shown in Fig. 17(a) and (b).

The phase current waveform and spectrum for the proposed 7LTHC method with measured speed under 2 Nm load torque are depicted in Fig. 18. Fig. 19 also shows the phase current waveform and spectrum for observed speed by SMO. While the THD is 7.59% in the measured speed condition, in the observed speed condition the THD is 7.95%. In other words, there has been an increase of 4.7% for THD in the observed speed condition according to the measured speed condition. However, it can be seen that the phase currents have nearly sinusoidal waveform as much as in the measured speed condition when the observed speed condition were applied.

The stator flux location in the stationary reference frame for the proposed 7LTHC method at operation condition, as shown Fig. 13, is presented in Fig. 20. The stator flux is circular by nature α-axis

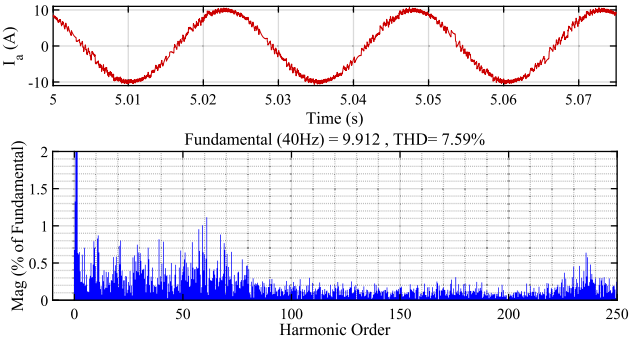

Fig. 18. Stator current and THDI for phase A under 2 Nm load at 1200 rpm with measured speed.

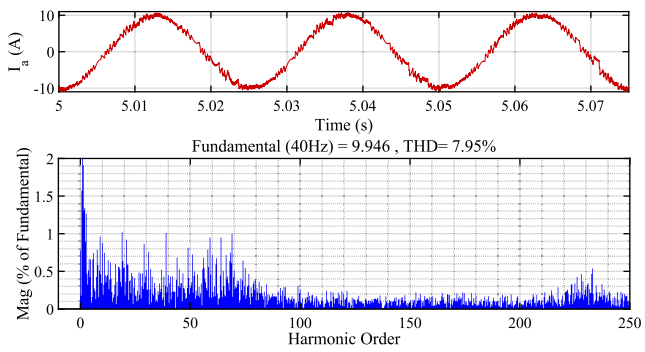

Fig. 19. Stator current and THDI for phase A under 2 Nm load at 1200 rpm with observed speed.

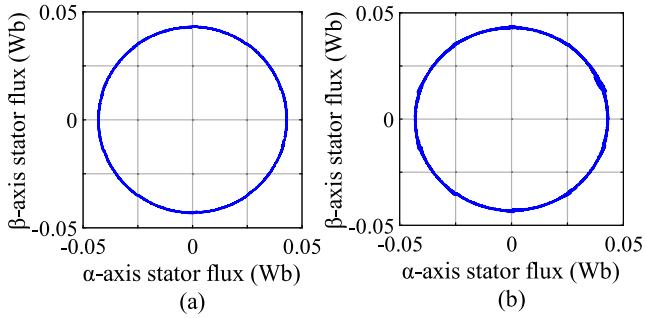

Fig. 20. Stator flux of α-β axis for proposed 7LTHC method. (a) with measured speed (b) with observed speed.

flux is quadrant to β-axis flux. Also, the stator flux is as smooth as a circle because of reducing flux ripples by the 7LTHC with the measured speed condition as shown in Fig. 20(a). As can been seen from Fig. 20(b), the shape of stator flux is nearly decagon due to the effect of chattering when the motor is accelerated from 600 rpm to 1200 rpm with the observed speed condition.

7. Conclusion

In this paper, the proposed 7LTHC is compared with the 3LTHCs that use of the voltage vector groups of the different amplitudes in terms of minimizing torque ripple and current distortion and dynamic torque response speed for five-phase IPMSM. The methods are implemented using Matlab/Simulink and tested under variable load and variable speed conditions. The amplitude of the voltage vector is directly related to the current ripple, and response time and ripple of the torque. The voltage vectors of the same amplitude can also have different response times due to the tangential component's magnitude for the same sector. Simulation results revealed that the 7LTHC that using the fast torque response vectors reduces both the torque ripple and current distortion in the steady-state while improving the torque response in the transient state. Meanwhile, the medium voltage vectors minimize torque ripples at the end of transient state conditions to eliminate the overshoot, while it can be increased torque ripples in the steady-state. Also, sigmoid function-based SMO combined with ATO is applied for sensorless speed control of the proposed 7LTHC method. The simulation results validate the SMO ensures to the estimation of precise rotor position as much as position sensors. In the future, this paper can be extended by investigating the effect of d3-q3 stator flux components when is used the 7LTHC that implements fast torque response vectors for sensorless applications.

Declaration of Competing Interest

The authors declare that they have no known competing financial interests or personal relationships that could have appeared to influence the work reported in this paper.

References

[1] S. Sadeghi, L. Guo, H.A. Toliyat, L. Parsa, Wide operational speed range of five-phase permanent magnet machines by using different stator winding configurations, IEEE Trans. Ind. Electron. 59 (6) (2011) 2621–2631, https://doi.org/10.1109/TIE.2011.2164771.
[2] C. Xue, S. Wensheng, F. Xiaoyun, Finite control-set model predictive current control of five-phase permanent-magnet synchronous machine based on virtual voltage vectors, IET Electric Power Applications 11 (5) (2017) 836–846, https://doi.org/10.1049/iet-epa.2016.0529.
[3] Y. Zhou, Z. Yan, Q. Duan, L. Wang, X. Wu, Direct torque control strategy of five-phase PMSM with load capacity enhancement, IET Power Electronics 12 (3) (2018) 598–606, https://doi.org/10.1049/iet-pel.2018.5203.
[4] L. Parsa, H.A. Toliyat, Sensorless direct torque control of five-phase interior permanent-magnet motor drivesIEEE Transactions on Industry applications (2007) 952–959, https://doi.org/10.1109/TIA.2007.900444.
[5] I. Takahashi, T. Noguchi, A new quick-response and high-efficiency control strategy of an induction motor, IEEE Transactions on Industry applications IA-22 (1986) 820–827, https://doi.org/10.1109/TIA.1986.4504799.
[6] L. Zhong, M.F. Rahman, W.Y. Hu, K.W. Lim, Analysis of direct torque control in permanent magnet synchronous motor drives, IEEE Transactions on Power Electronics 12 (3) (1997) 528–536, https://doi.org/10.1109/63.575680.
[7] S. Vaez-Zadeh, E. Jalali, Combined vector control and direct torque control method for high performance induction motor drives, Energy conversion and management 48 (12) (2007), https://doi.org/10.1016/j.enconman.2007.05.010.
[8] H.A. Toliyat, H. Xu, A novel direct torque control (DTC) method for five-phase induction machines, In: Fifteenth Annual IEEE Applied Power Electronics Conference and Exposition. APEC 2000, New Orleans, LA, USA, 2000. pp. 162-168. https://doi: 10.1109/APEC.2000.826100.
[9] K.B. Lee, J.H. Song, I. Choy, J.Y. Yoo, Torque ripple reduction in DTC of induction motor driven by three-level inverter with low switching frequency, IEEE Trans. Power Electron. 17 (2) (2002) 255–264, https://doi.org/10.1109/63.988836.
[10] L. Parsa, On advantages of multi-phase machines, In: 31st Annual Conference of IEEE Industrial Electronics Society, IECON, Raleigh, NC, USA, 2005, p. 6, https://doi.org/10.1109/IECON.2005.1569139.
[11] L. Zheng, J.E. Fletcher, B.W. Williams, X. He, A novel direct torque control scheme for a sensorless five-phase induction motor drive, IEEE Transactions on Industrial Electronics 52 (2) (2010) 503–513, https://doi.org/10.1109/TIE.2010.2047830.
[12] L. Gao, J.E. Fletcher, L. Zheng, Low-speed control improvements for a two-level five-phase inverter-fed induction machine using classic direct torque control, IEEE Transactions on Industrial Electronics 58 (7) (2010) 2744–2754, https://doi.org/10.1109/TIE.2010.2070775.
[13] Y. Tatte, M. Aware, Torque ripple reduction in direct torque controlled five-phase induction motor using modified five-level torque comparator, Sādhanā. 43 (1) (2018) 6, https://doi.org/10.1007/s12046-017-0767-9.
[14] Y.N. Tatte, M.V. Aware, Torque ripple reduction in five-phase direct torque controlled induction motor, In: 2014 IEEE international conference on power electronics, drives and energy systems. PEDES, Mumbai, India, 2014. pp. 1-5. URL: https://doi: 10.1109/PEDES.2014.7042048.
[15] Y. Gao, L. Parsa, Modified direct torque control of five-phase permanent magnet synchronous motor drives, In: APEC 07-Twenty-Second Annual IEEE Applied Power Electronics Conference and Exposition, Anaheim, CA, USA, 2007. pp. 1428-1433. URL: https://doi: 10.1109/APEX.2007.357704.
[16] B. Cao, B.M. Grainger, X. Wang, Y.u. Zou, G.F. Reed, Z.H. Mao, Direct torque model predictive control of a five-phase permanent magnet synchronous motor, IEEE Trans. Power Electron. 36 (2) (2021) 2346–2360, https://doi.org/10.1109/TPEL.2020.3011312.
[17] G. Liu, Y. Yang, Q. Chen, Virtual signal injected MTPA control for DTC five-phase IPMSM drives, Journal of Power Electronics 19 (4) (2019) 956–967, https://doi.org/.
[18] K. Tondpoor, S.M. Saghaiannezhad, A. Rashidi, Sensorless control of PMSM Using Simplified Model Based On Extended Kalman filter. In: 2020 11th Power Electronics, Drive Systems, and Technologies Conference. PEDSTC, Tehran, Iran. pp. 1-5. IEEE. URL: https://doi: 10.1109/PEDSTC49159.2020.9088400.
[19] S. Fabbri, S. Catalano, M. Palmieri, F. Cupertino, M. Nienhaus, E. Grasso, Full speed range sensor less control for PMSM using an adaptive extended Kalman filter. In: 2020 AEIT International Annual Conference. AEIT, Catania, Italy, 2020. pp. 1-6. IEEE. URL: https://doi: 10.23919/AEIT50178.2020.9241112.
[20] Y. Zhu, B. Tao, M. Xiao, G. Yang, X. Zhang, K.e. Lu, Luenberger Position Observer Based on Deadbeat-Current Predictive Control for Sensorless PMSM, Electronics. 9 (8) (2020) 1325, https://doi.org/10.3390/electronics9081325.
[21] Y. Xing, X. Wang, D. Yang, Z.M. Zhang, Sensorless control of permanent magnet synchronous motor based on model reference adaptive system. In: 2017 10th

International Symposium on Computational Intelligence and Design. ISCID, Hangzhou, China, 2017. Vol. 1, pp. 20-23. IEEE. URL: https://doi: 10.1109/ISCID.2017.17.

[22] A.G. Abo-Khalil, A.M. Eltamaly, M.S. Alsaud, K. Sayed, A.S. Alghamdi, Sensorless control for PMSM using model reference adaptive system, International Transactions on Electrical Energy Systems. e12733 (2020), https://doi.org/10.1002/2050-7038.12733.

[23] S. Lin, W. Zhang, An adaptive sliding-mode observer with a tangent function-based PLL structure for position sensorless PMSM drives, Int. J. Electr. Power Energy Syst. 88 (2017) 63–74, https://doi.org/10.1016/j.ijepes.2016.12.006.

[24] S. Chen, X. Zhang, X. Wu, G. Tan, X. Chen, Sensorless control for IPMSM based on adaptive super-twisting sliding-mode observer and improved phase-locked loop, Energies. 12 (7) (2019) 1225, https://doi.org/10.3390/en12071225.

[25] X. Sun, J. Cao, G. Lei, Y. Guo, J, Zhu, Speed sensorless control for permanent magnet synchronous motors based on finite position set, IEEE Transactions on Industrial Electronics. 67 (7) (2019) 6089–6100, https://doi.org/10.1109/TIE.2019.2947875.

[26] X. Sun, C. Hu, G. Lei, Z. Yang, Y. Guo, J. Zhu, Speed sensorless control of SPMSM drives for EVs with a binary search algorithm-based phase-locked loop, IEEE Trans. Veh. Technol. 69 (5) (2020) 4968–4978, https://doi.org/10.1109/TVT.2020.2981422.

[27] J. Liu, T.A. Nondahl, P.B. Schmidt, S. Royak, M. Harbaugh, Rotor Position Estimation for Synchronous Machines Based on Equivalent EMF, IEEE Transactions on Industry Applications 47 (3) (2011), https://doi.org/10.1109/TIA.2011.2125935.

[28] W. Lu, Z. Zhang, D. Wang, K. Lu, D. Wu, K. Ji, L. Guo, A new load torque identification sliding mode observer for permanent magnet synchronous machine drive system, IEEE Trans. Power Electron. 34 (8) (2019) 7852–7862, https://doi.org/10.1109/TPEL.2018.2881217.

[29] A. Hosseyni, R. Trabelsi, M.F. Mimouni, A. Iqbal, R. Alammari, Sensorless sliding mode observer for a five-phase permanent magnet synchronous motor drive, ISA Transactions 58 (2015) 462–473, https://doi.org/10.1016/j.isatra.2015.05.007.

[30] Y. Mini, N.K. Nguyen, E. Semail, Sensorless control for non-sinusoidal five-phase observer IPMSM based on sliding mode observer, In: 2019 Jeunes Chercheursen Génie Electrique, SEEDS, Oléron, France, 2019, pp. 1–10.

[31] F. Niu, B. Wang, A.S. Babel, K. Li, E.G. Strangas, Comparative evaluation of direct torque control strategies for permanent magnet synchronous machines, IEEE Trans. Power Electron. 31 (2) (2015) 1408–1424, https://doi.org/10.1109/TPEL.2015.2421321.

[32] Z. Qiao, T. Shi, Y. Wang, Y. Yan, C. Xia, X. He, New Sliding-Mode Observer for Position Sensorless Control of Permanent-Magnet Synchronous Motor, IEEE Trans. Ind. Electron. 60 (2) (2013) 710–719, https://doi.org/10.1109/TIE.2012.2206359.

[33] H. Kim, J. Son, J. Lee, A High-Speed Sliding-Mode Observer for the Sensorless Speed Control of a PMSM, IEEE Transactions on Industrial Electronics 58 (9) (2011) 4069–4077, https://doi.org/10.1109/TIE.2010.2098357.

[34] Y. Zhao, W. Qiao, L. Wu, Position extraction from a discrete sliding-mode observer for sensorless control of IPMSMs, In: 2012 IEEE International Symposium on Industrial, Electronics, Hangzhou, China, 2012, pp. 725–730, https://doi.org/10.1109/ISIE.2012.6237159.

[35] L. Guo, L. Parsa, Model reference adaptive control of five-phase IPM motors based on neural network, IEEE Transactions on Industrial Electronics (2011) 1500–1508, https://doi.org/10.1109/TIE.2011.2163371.

[36] Y. Ren, Z.Q. Zhu, Reduction of both harmonic current and torque ripple for dual three-phase permanent-magnet synchronous machine using modified switching-table-based direct torque control, IEEE Trans. Ind. Electron. 62 (11) (2015) 6671–6683, https://doi.org/10.1109/TIE.4110.1109/TIE.2015.2448511.